Available online at www.sciencedirect.com
ScienceDirect
Biomaterials 28 (2007) 1741–1751
Biomaterials
www.elsevier.com/locate/biomaterials

# Synthesis and characterization of electroactive and biodegradable ABA block copolymer of polylactide and aniline pentamer

Lihong Huang[a,b], Jun Hu[a,b], Le Lang[a,b], Xin Wang[a], Peibiao Zhang[a], Xiabin Jing[a], Xianhong Wang[a], Xuesi Chen[a,*], Peter I. Lelkes[c], Alan G. MacDiarmid[d], Yen Wei[c,**]

[a]*State key Laboratory of Polymer Physics and Chemistry, Changchun Institute of Applied Chemistry, Chinese Academy of Sciences, Changchun 130022, China*
[b]*Graduate School of Chinese Academy of Sciences, Beijing 100039, China*
[c]*Department of Chemistry and School of Biomedical Engineering, Drexel University, Philadelphia, PA 19104, USA*
[d]*Department of Chemistry, University of Pennsylvania, Philadelphia, PA 19104, USA*

Received 11 July 2006; accepted 1 December 2006
Available online 10 January 2007

**Abstract**

A triblock copolymer PLA-*b*-AP-*b*-PLA (PAP) of polylactide (PLA) and aniline pentamer (AP) with the unique properties of being both electroactive and biodegradable is synthesized by coupling an electroactive carboxyl-capped AP with two biodegradable bi-hydroxyl-capped PLAs via a condensation reaction. Three different molecule weight PAP copolymers are prepared. The PAP copolymers exhibit excellent electroactivity similar to the AP and polyaniline, which may stimulate cell proliferation and differentiation. The electrical conductivity of the PAP2 copolymer film ($\sim 5 \times 10^{-6}$ S/cm) is in the semiconducting region. Transmission electron microscopic results suggest that there is microphase separation of the two block segments in the copolymer, which might contribute to the observed conductivity. The biodegradation and biocompatibility experiments *in vitro* prove the copolymer is biodegradable and biocompatible. Moreover, these new block copolymer shows good solubility in common organic solvents, leading to the system with excellent processibility. These biodegradable PAP copolymers with electroactive function thus possess the properties that would be potentially used as scaffold materials for neuronal or cardiovascular tissue engineering.


*Keywords:* Electroactive; Biodegradable; Polylactide; Aniline pentamer; Biocompatibility

## 1. Introduction

Polyaniline is one of the most promising electrically conductive polymers because of its unique properties, including controllable electrical conductivity, environmental stability and rich redox chemistry, and its numerous potential applications, such as anticorrosion coatings [1,2], batteries [3–5], sensors [6,7], separation membranes [8–10], antistatic coatings [11,12] and electromagnetic interference shielding [13,14].

Recently, polyaniline has been explored for applications as novel intelligent scaffolds for cardiac and/or neuronal tissue engineering [15–20]. The basic idea was that the cell proliferation, assembly, and particularly, differentiation might be influenced, directed or even controlled by electrical or electrochemical stimulation applied through the electroactive scaffold materials. Past work has demonstrated that electrical charges play an important role in stimulating either the proliferation or differentiation of various cell types, and electrically conducting or electroactive polymers provide potentially interesting surfaces for cell culture in that their properties (e.g., surfaces charge, wettability, and conformational and dimensional changes) can be altered reversibly by chemical or electrochemical oxidation or reduction [21,22]. Recent studies have demonstrated that polyaniline and its derivatives can

*Corresponding author. Tel.: +86 431 5262112; fax: +86 431 5685653.
**Also to be corresponded at. Tel: +1 215 895 2650; fax: +1 215 895 1265.
*E-mail addresses:* xschen@ciac.jl.cn (X. Chen), yenwei@drexel.edu (Y. Wei).

0142-9612/$ - see front matter © 2006 Elsevier Ltd. All rights reserved.
doi:10.1016/j.biomaterials.2006.12.007

function as biocompatible substrates, upon which both H9c2 cardiac myoblasts and PC12 pheochromocytoma cells were found to adhere, grow and/or differentiate well [17–20]. Other electroactive polymers, such as polypyrrole, were shown to enhance the effect of nerve growth factor (NGF) in inducing neuronal differentiation of PC 12 cells with electric stimulation [23].

One of the primary factors of application of conducting polymers in biotechnology is the poor polymer–cell interaction. The biocompatibility of electroactive polymers can be improved by blending with bioactive materials, grafting biocompatible side chains onto the surface or covalently bonding some biocompatible segments in the main chain of the polymers. For example, polyanline was blended with natural polymers such as collagen [15] and gelatin [24,25] or covalently grafted with oligopeptides such as Tyr–Ile–Gly–Ser–Arg (YIGSR) [17–20]. Rivers et al. [26] introduced ester linkages into the backbone structure of pyrrole oligomers. Another severe problem that hinders the applications of conducting polymers is the poor solubility and processibility [27]. The solubility of polyaniline could be enhanced by covalently grafting side groups or polymers, such as poly(ethylene glycol) [28] and poly(acrylic acid) [29], on the backbone of polyaniline.

Despite all the above-mentioned success, one of the most important issues related to the applications of electroactive polymers as tissue engineering scaffolds is the lack of biodegradability for the conducting polymers, which prohibits *in vivo* applications. Keeping conductive polymers such as polyaniline in the body for a long time may induce chronic inflammation and require surgical removal. Therefore, to introduce biodegradability to conductive polymers is a very important and challenging task.

We envisioned that a block copolymer having biodegradable polymer segments covalently bonded to an electroactive polymer segment such as polyaniline could exhibit improved biocompatibility, biodegradability, solubility and processability of electroactive biomaterials. We selected polylactide (PLA) as the biodegradable segment for its proved biocompatibility and biodegradability, and the low-molecular-weight aniline pentamer (AP) as the electroactive segment for its reasonably good solubility and comparable electroactivity as polyaniline [30,31]. In addition, after the degradation of the block copolymer, it is possible that the degradation product AP could be consumed by macrophages during the normal wound healing response, reducing chances of long term and adverse responses [26,32].

In this study, PLA-*b*-AP-*b*-PLA (PAP) triblock copolymer with good electroactivity and biodegradability was designed and synthesized by the co-condensation of one bi-carboxyl-capped AP and two bi-hydroxyl-capped PLA initiated by butanediol in the presence of *N*,*N*′-dicyclohexylcarbodiimede (DCC) as the dehydrating agent. The AP is the hard segment in the copolymer due to the inflexibility of benzene rings and the $\pi$-conjugation system, while the chains of PLA are the soft and flexible segments in the copolymer. The PAP copolymer has potential applications as biodegradable scaffolds for neuronal and cardiovascular tissue engineering, drug release carriers, biosensors and other biomedical devices that require electroactivity.

## 2. Materials and methods

### 2.1. Materials

*N*-methyl-pyrrolidome (NMP) and toluene were distilled after drying with $CaH_2$. *N*,*N*-dimethylformamide (DMF), tetrahydrofuran (THF), methylene chloride ($CH_2Cl_2$), chloroform ($CHCl_3$), 1,2-ethylene chloride, and hydrochloric acid (HCl) were used as received. 1,4-Butanediol (BDO), stannous octoate [$Sn(Oct)_2$, 95%], *p*-phenylenediamine, *N*-phenyl-1,4-phenylenediamine, *N*,*N*′-dicyclohexyl carbodiimide (DCC), 4-dimethylaminopyridine (DMAP), butane diacid anhydride, camphorsulfonic acid (CSA) and ammonium persulfate were purchased from Aldrich and were used as received without further purification. Lactide was purchased from Purac, Holland.

### 2.2. Synthesis of the PAP block copolymer

#### 2.2.1. Hydroxyl-capped PLA (PLA) (see step 1 in Scheme 1)

After recrystallization in ethyl acetate for three times, lactide was added to a flame-dried and nitrogen-purged glass ampoule, into which a toluene solution of BDO and $Sn(Oct)_2$ (0.3% of the BDO, mol/mol) was then transferred. The reaction vessel was immersed into a thermostatic oil bath maintained at 125 °C, under magnetic stirring for 24 h. The reaction product was precipitated into ethanol, filtered and dried at 40 °C in vacuum for 48 h [33].

*Characterization*: $^1$H NMR (400 MHz, $CDCl_3$) $\delta$ 5.16 (t, 2H, poly –CH), 4.39 (t, 2H, end –CH), 4.19 (s, 4H, $-CH_2-$), 1.61 (d, 6H, poly $-CH_3$), 1.51 (d, 6H, end $-CH_3$). $^{13}$C NMR (100 MHz, DMSO-$d_6$) $\delta$ 169.67 (end –CO–), 169.16 (poly –CO–), 68.67 (poly –CH), 67.74 (end –CH), 64.50 ($-CH_2-$), 24.46 ($-CH_2-$), 20.29 (end $-CH_3$), 16.42 (poly $-CH_3$). IR (neat, $cm^{-1}$) 3512 (m, $\nu_{OH}$), 3000 (w, $\nu_{as}$ CH3), 2950 (w, $\nu_{OH}$), 1761 (s, $\nu_{C=O}$), 1454 (s, $\delta_s$ $CH_3$), 1393 (w, $\delta_{as}$ $CH_3$), 1377, 1363 (w, $\delta_s$ C–$CH_3$), 1185, 1087 (m, $\nu_{O-C-O}$), 879, 760 (s, $\gamma$ C–$CH_3$).

#### 2.2.2. Carboxyl-capped aniline pentamer (AP) (see step 2 in Scheme 1)

The synthesis of AP was based on the method reported in the literature [34,35]. *p*-Phenylenediamine and *N*-phenyl-1,4-phenylenediamine whose amino group was protected with butane diacid anhydride were dissolved in the mixture solution of DMF and hydrochloric acid (HCl). The emeraldine (EM) base form of AP was obtained upon addition of ammonium persulfate as the oxidant at room temperature under stirring. Then, the fully reduced leucoemeraldine (LM) of AP was prepared by reducing the EM base with hydrogen at 3 atmospheres over platinum oxide for 2 h [36]. Under protection of nitrogen, the light gray LM AP product was washed thoroughly with distilled water till the filtrate became colorless, followed by washing in a Soxhlet extractor with 1,2-dichloroethane and THF to remove the excess reducing agent and by-products in reactions. The LM AP powders were then dried under reduced pressure.

*Characterization*: $^1$H NMR (400 MHz, DMSO-$d_6$) $\delta$ 12.00 (s, 2H, –COOH), 9.70 (s, 2H, –CO–NH–), 7.62 (s, 2H, –NH–), 7.50 (s, 2H, –NH–), 7.37 (d, 4H, Ar–H), 6.94–6.85 (m, 16H, Ar–H). $^{13}$C NMR (100 MHz, DMSO-$d_6$) $\delta$ 177.23 (–COOH), 173.96 (–CO–NH–), 140.79 (Ar–C), 138.30 (Ar–C), 137.11 (Ar–C), 135.65 (Ar–C), 132.35 (Ar–C),120.42 (Ar–C), 119.50 (Ar–C), 118.34 (Ar–C), 117.49 (Ar–C), 115.36 (Ar–C), 31.01 ($-CH_2-$), 29.20 ($-CH_2-$). IR (neat, $cm^{-1}$) 3409 (m, $\nu_{NH}$), 3273 (m, $\nu_{NH}$), 1707 (s, $\nu_{C=O}$), 1507 (s, $\nu_{C=C}$ of benzenoid rings). Mass spectrometry: 672.5 ($MH^+$/e). Anal. Calcd for $C_{38}H_{36}N_6O_6$: C, 67.84; H, 5.39; N, 12.49; O, 14.27. Found: C, 67.63; H, 5.40; N, 12.58; O, 13.87.

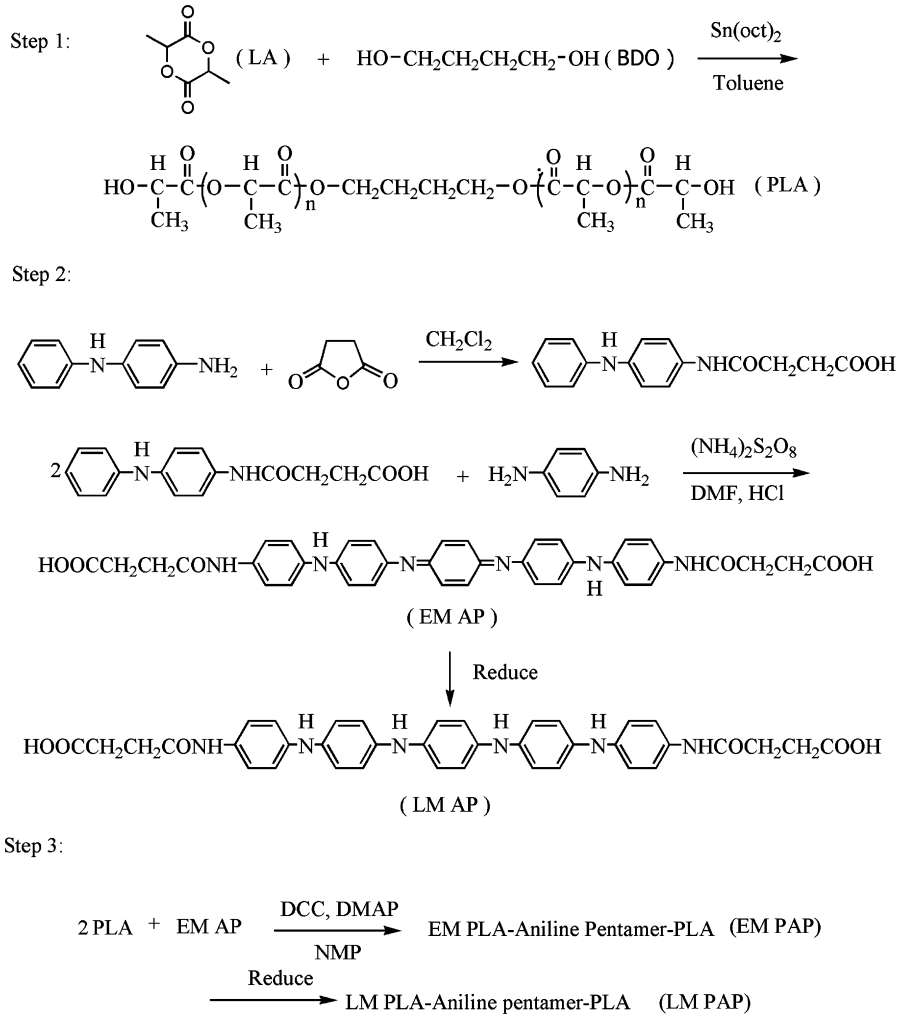


Scheme 1. Schematic diagram illustrating the synthesis of the LM PAP copolymer.

*2.2.3. Synthesis of triblock PAP copolymer (see step 3 in Scheme 1)*

In order to avoid the influence of the low molecular compounds such as ethanol and $H_2O$, the hydroxyl-capped PLA (PLA) was azeotropically distilled in toluene for 18 h first. Then 2 mmol purified PLA, 1 mmol emeraldine of carboxyl-capped aniline pentamer (EM AP), 5 mmol DCC, 5 mmol DMAP and 15 ml NMP were added into a flame-dried glass reactor. After nitrogen-purged three times, the reactor was then sealed and cooled to 0 °C for 48 h with magnetic stirring [37]. After the reaction, dicyclohexylurea was removed by filtration. The copolymer in the filtrate was precipitated in ethanol and was dissolved in $CHCl_3$, followed by precipitation in ethyl ether again. Such a dissolution-precipitation process was repeated three times to purify the product. The final product, emeraldine of the copolymer (EM PAP) was dried under vacuum at room temperature for 24 h. The synthesis of the fully reduced leucoemeraldine of the copolymer (LM PAP) from EM PAP was achieved by following the same procedures as in the preparation of the LM AP as described earlier.

*Characterization*: $^1$H NMR (400 MHz, DMSO-$d_6$) $\delta$ 9.72 (s, 2H), 7.62 (s, 2H), 7.51 (s, 2H), 7.35 (d, 4H), 6.94–6.84 (m, 16H) for AP segment, and 5.17 (t, 2H, poly), 4.21 (t, 2H), 4.10 (s, 4H), 1.47 (d, 6H, poly), 1.28 (d, 6H) for PLA segments. $^{13}$C NMR (100 MHz, DMSO-$d_6$) $\delta$ 173.97 (–CO–NH–), 171.85 (–CO–O–), 169.14 (poly –CO–), 140.88 (Ar–C), 138.32 (Ar–C), 137.09 (Ar–C), 135.58 (Ar–C), 130.58 (Ar–C), 120.44 (Ar–C), 119.53 (Ar–C), 118.32 (Ar–C), 117.46 (Ar–C), 115.29 (Ar–C), 68.64 (poly –CH–), 67.71 (end –CH–), 64.48 (–$CH_2$–), 30.32 (–$CH_2$–), 28.51 (–$CH_2$–), 24.32 (–$CH_2$–), 20.28 (end –$CH_3$), 16.41 (poly –$CH_3$). IR (neat, $cm^{-1}$) 2999 (w, $\nu_{as}$ $CH_3$), 2945 (w, $\nu_{OH}$), 1759 (s, $\nu_{C=O}$ for ester bond), 1670 (m, $\nu_{C=O}$ for amide bond), 1503 (s, $\nu_{C=C}$ of benzenoid rings), 1450 (s, $\delta_s$ $CH_3$), 1388 (w, $\delta_{as}$ $CH_3$), 1360 (w, $\delta_s$ C–$CH_3$), 1187, 1093 (m, $\nu_{O-C-O}$), 868, 755 (s, $\gamma$ C–$CH_3$).

## 2.3. Preparation of copolymer thin films

The copolymer samples were dissolved in $CHCl_3$ to form 5 wt% solutions. The solutions were cast onto a super-flat glass culture plates and placed for 5 h under room temperature to form thin films. The films thus obtained were dried under reduced pressure at room temperature for 48 h to remove $CHCl_3$.

## 2.4. Conductivity measurements

To prepare the copolymer film for conductivity measurement, a solution of PAP2 copolymer doped with CAS in $CHCl_3$ (~0.1 g/ml) was dropped onto the center of a polytetrafluoroethylene plate and was evaporated at room temperature to form thin film. The films were dried under reduced pressure at room temperature for 48 h, then cut into a square. The standard Van Der Pauw DC four-probe method was used to measure the electrical conductivity of the PAP2 copolymer. The square was placed on the four-probe apparatus. Providing a voltage, a corresponding electrical current could be obtained. The electrical conductivity of samples was calculated by the following formula: $\sigma$ ($S$/cm) = $(2.44 \times 10/S) \times (I/E)$, where $\sigma$ is the conductivity; $S$ is the sample side area;

$I$ is the current passed through outer probes; $E$ is the voltage drop across inner probe.

### 2.5. Degradation of copolymers

For PAP1, PAP2 and PAP3 copolymers, three specimens ($10 \times 10 \times 0.4$ mm) of each copolymer made from films were placed in tubes filled with phosphate buffer (pH = 7.4). The tubes were placed in the thermostatic shaker at 37 °C. After different time, the specimens were taken out and washed with distilled water, then dried at room temperature in vacuum for 1 week before being subjected to loss weight analysis. The loss weight is gained from the average value of three samples.

### 2.6. Cell adhesion and proliferation

The PAP2 copolymer was dissolved in chloroform to form a 1 wt% solution. The solution (50 μl) was coated onto a 24 mm × 24 mm cover-slide (treated with 2% dimethyl dichlorosilane (Fluka)/chloroform solution in order to improve the contact angle and make the copolymer attach the cover-slide more easily, then dried at 180 °C for 4 h before use) and the solvent was removed by drying in the air for 30 min and following dry in vacuum for 48 h at room temperature. The cover slides were sterilized with UV for 30 min. Rat C6 glioma cells were used to investigate the cell adhesion and viability of PAP2 copolymer. The cells were rinsed three times with 0.1 M PBS by centrifugation at 15 000 rpm for 5 min, and cultured in cell culture flasks in a density of $2.0 \times 10^4/cm^2$ with RPMI 1640 medium (GIBCO) supplemented with 10% fetal calf serum (GIBCO), $1.0 \times 10^5$/l penicillin (SIGMA) and 100 mg/l Streptomycin (SIGMA), in a humidified incubator at 37 °C and 5% $CO_2$. The medium was changed every 2 days. After 3–5 days culture, the monolayer C6 cells were removed from the cell culture flasks by trypsin (2.5 ml/ml) treatment, rinsed three times with 0.1 M PBS by centrifugation at 1500 rpm for 5 min. The obtained C6 cells were re-suspended in the medium to adjust cell density to $1.0 \times 10^5$ cells/well (in 1 ml of medium), then seeded on the cover-slides coated with the PAP2 copolymer which were placed into 6-well plates (Costar) and tissue-culture-treated polystyrene (TCPS) (the empty 6-well plates) before sterilized with UV for 30 min and washed three times with PBS. Three milliliters of medium were added into each well to prevent the cove-slide from floating during cells seeding. The plates were incubated at 37 °C and 5% $CO_2$ for 4 and 48 h [38]. The cover-slides were washed three times with PBS, and fixed with 3% glutaraldehyde in PBS at room temperature for 30 min, washed with distilled water, and dried in air. Cell attachment and proliferation were observed under the reverse microscope (TE2000U, NIKON). The pictures were taken by DIGITAL CAMERA DXM1200F (NIKON), and analyzed with NIH Image *J*, area fraction of cells in each cover-slide was obtained.

### 2.7. Characterization

FT-IR spectra of the PAP powders were recorded on a Bio-Rad Win-IR instrument. $^{13}C$ nuclear magnetic resonance (NMR) spectra were recorded on a Bruker AV 100 MHz spectrometer with DMSO-$d_6$ as the solvent at room temperature. Matrix-assisted laser desorption/ionization time-of-flight (MALDI-TOF) mass spectra were performed on an AXIMA-CFR laser desorption ionization time-of-flight spectrometer (COMPACT). Gel permeation chromatography (GPC) measurements were carried out at 35 °C with a Waters 505 GPC instrument equipped with three Waters Styragel columns (HT3, HT4 and HT5) and a differential refractometer detector. $CHCl_3$ was used as an eluent at a flow rate of 1 ml/min. The molecular weights were calibrated with polystyrene standards. The UV–visible spectra of the copolymer solutions were monitored on a UV–vis spectrophotometer (UV-2401). Samples for cyclic voltammetry were prepared by depositing thin LM PAP film on an indium tin oxide (ITO) electrode as working electrode and $Ag/Ag^+$ as reference electrode. Cyclic voltammograms were recorded on a CHI 630 potentiostat with a scanning rate of 100 mV/s. The electrical conductivity of the EM PAP films doped with camphorsulfonic acid was measured by the four-probe method. The phase separation of LM PAP was studied by transmission electron microscopy (TEM), using a JEOL JEM-1010 electron microscope. The film of LM PAP which had been embedded in epoxide resin was frozen with liquid nitrogen and cut into thin segment of 60–80 nm in thickness by the Leica CM1100 Cryostat Microtome, then, was examined with TEM. The TEM measurements were performed at an accelerating voltage of 100 kV.

## 3. Results and discussion

### 3.1. Synthesis

The schematic procedures of the synthesis of the PAP copolymer are shown in Scheme 1. The results of copolymer compositions, molecular weights from proton nuclear magnetic resonance ($^1H$ NMR) and gel permeation chromatography (GPC), respectively, are summarized in Table 1. The molecular weights of PLA determined from $^1H$ NMR were used in the calculation of reactant feed ratios in the synthesis of block copolymers. The feed molar ratios for the preparation of the copolymers PAP1, PAP2 and PAP3 were kept the same at 1:2 and the difference among them was the different molecular weights of PLA employed. For PAP1, PAP2 and PAP3, the number-average molecular weights of PLA were 1.0, 2.8 and 4.7 k, respectively. Therefore, the weight fraction of aniline-pentamer at the emeraldine oxidation state (EM AP) in the copolymer decreased with the increase of the PLA molecular weight. Based on the comparison of the molecular weights of PLAs with the PAP copolymers, these three copolymer samples all had molecular weights greater than twice of the corresponding PLA prepolymers and hence were consistent with the proposed triblock copolymers of PAP. In the synthesis, we had to control the mole number of PLA to be twice of that of the AP in order to obtain the triblock copolymers. The polydispersity indexes (PDI) of all the starting PLA materials and the resultant copolymers were in a relatively narrow range of 1.02–1.24. The PDIs for the PLA precursors were generally smaller than those of the corresponding copolymers.

The success of the synthesis and the structure of PAP triblock copolymers were further demonstrated by NMR analysis. In order to gain simple and clear NMR spectra, the copolymers in fully reduced form, i.e., leucoemeraldine (LM) of AP, were used in the $^{13}C$ NMR measurements to avoid the complications from quinoid signals in the EM copolymer spectra. Fig. 1 shows a representative $^{13}C$ NMR (100 MHz, DMSO-$d_6$) spectrum of LM PAP2 with several regions expanded for better viewing. The peaks of PAP2 labeled in corresponding positions on the structures are in accordance with the characteristic peaks of LM AP and PLA. The appearance of new peak 1 indicates the formation of new ester bond from the condensation of terminal carboxyl groups of AP and terminal hydroxyl group of PLA. In the $^1H$ NMR (400 MHz, DMSO-$d_6$) spectrum of PAP2, the peak area $\delta$ 4.104 (–$CH_2$– in the butanediol unit of PLA segment) was about fourfold of the

Table 1
Composition and GPC data of the PAP copolymers

| Samples | Feed mol. ratio[a] | Mol. wt. of PLA[b] (k) | Wt. frac. of EM AP (%)[c] | GPC of PLA | | | GPC of copolymers | | |
|---|---|---|---|---|---|---|---|---|---|
| | | | | Mw (k) | Mn (k) | PDI | Mw (k) | Mn (k) | PDI |
| PAP1 | 1:2 | 1.0 | 33.6 | 0.92 | 0.90 | 1.02 | 2.98 | 2.73 | 1.09 |
| PAP2 | 1:2 | 2.8 | 12.0 | 3.12 | 2.92 | 1.07 | 6.71 | 5.69 | 1.18 |
| PAP3 | 1:2 | 4.7 | 7.2 | 5.72 | 5.42 | 1.05 | 12.41 | 10.01 | 1.24 |

[a]Ratio of PLA to EM AP unit.
[b]Molecular weight of PLA, calculated from $^1$H NMR.
[c]Weight fraction of EM AP in the copolymers, calculated according to the molecular weight of PLA.

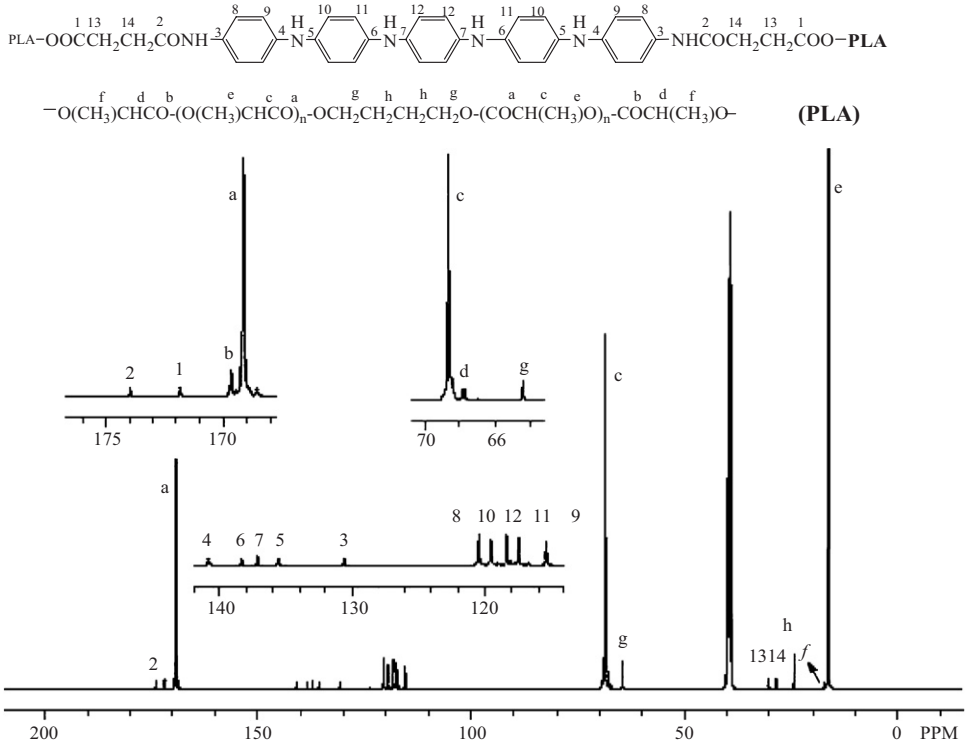


Fig. 1. $^{13}$C NMR spectrum (100 MHz, DMSO-$d_6$) of triblock PAP2 in respective regions.

peak area $\delta$ 9.717 (–NH two center units in the AP segment) meaning that one AP segment had 2H (–NH, $\delta$ 9.717) and two PLA segments had 8 H (–$CH_2$–, $\delta$ 4.104), which are consistent with the PAP triblock structure of the copolymer.

### 3.2. Solubility of the PAP copolymer samples

The solubility results for AP, PLA and PAP copolymers are summarized in Table 2. The AP sample could be only dissolved in strong polar solvents, such as DMF, DMSO and NMP. The PLA samples had excellent solubility in most of organic solvents. All the PAP copolymers exhibited excellent solubility in most of organic solvents just like PLA, which can be explained as that the soluble PLA chains bonded on the both ends of AP segment in the copolymers significantly improved the solubility of the electroactive AP segment.

### 3.3. Electrochemical characterization of the PAP copolymers

The PAP copolymers with the AP in EM form were blue, while their fully reduced LM forms were light gray. The color change of the copolymers indicated the conversion of the different oxidation states of AP unit in the PAP copolymers. The [ = N–]/[–NH–] ratios can be used to represent the oxidation states of polyaniline and aniline oligomers [28], which could be evaluated by FT-IR and UV–visible absorption spectroscopy. Fig. 2 shows the FT-IR spectra of EM AP, EM PAP2 and LM PAP2 powders. The absorption peaks at 1509 and 1587 cm$^{-1}$ could be attributed to the benzenoid unit and quonoid unit of the

Table 2
Solubility of AP, PLA and PAP copolymer samples

| Samples | Solvents | | | | | |
|---|---|---|---|---|---|---|
| | DMF | DMSO | NMP | $CHCl_3$ | THF | Toluene |
| AP | S | S | S | SS | I | I |
| PLA | S | S | S | S | S | S |
| PAP | S | S | S | S | S | S |

Key: S, soluble (up to a concentration of at least 1 g/100 ml); SS, slightly soluble; I, insoluble.

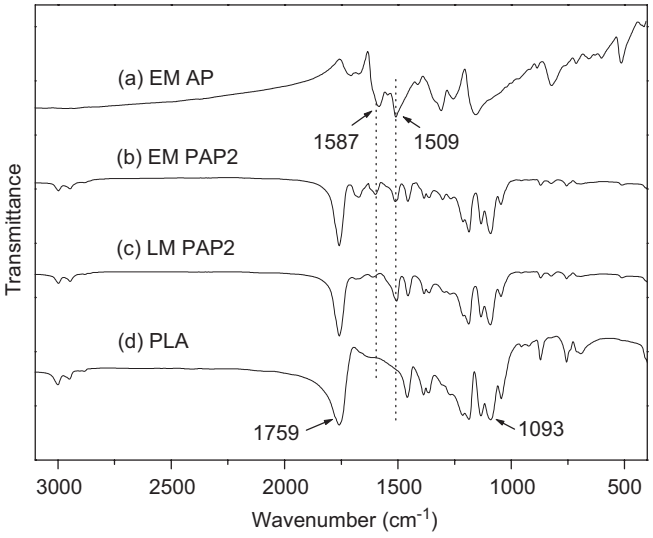


Fig. 2. FT-IR spectra of: (a) the EM AP powder, (b) the EM PAP2 copolymer power, (c) the LM PAP2 copolymer powder, and (d) pure PLA.

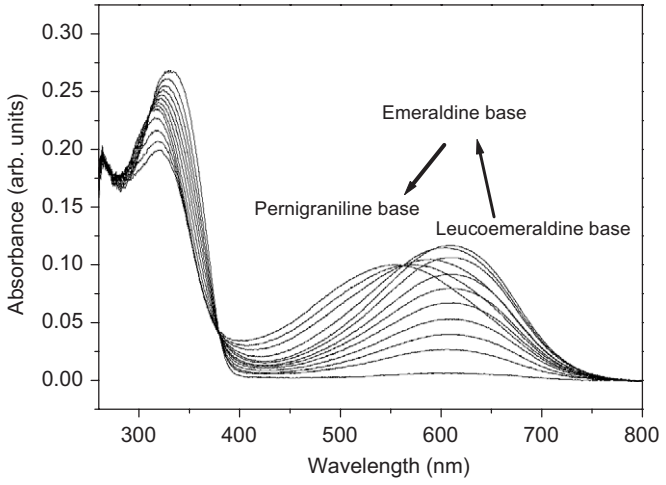


Fig. 3. The UV–vis spectra of PAP2 copolymer from leucoemeraldine base to emeraldine base, then to pemigraniline base in DMF oxidized with ammonium persulfate.

AP segment, respectively [39]. The intensities of the absorption band at 1587 $cm^{-1}$ for the EM AP is approximately half of the one at 1509 $cm^{-1}$, which are consistent with a third intrinsically oxidized AP structure. The spectrum of the EM copolymer sample shows similar bands as the EM AP sample at 1509 and 1587 $cm^{-1}$. The new peaks at 1093 and 1759 $cm^{-1}$ are from the C–O–C stretching and the C = O stretching vibrations in the PLA segments, which are the same as in the spectra of PLA. On the other hand, the predominance of the absorption band at 1509 $cm^{-1}$ to over that at 1587 $cm^{-1}$ for the LM copolymers indicates the success in reducing the AP segment from EM to LM oxidation state.

Fig. 3 shows the UV–visible absorption spectra of PAP2 in DMF. The UV–visible spectra of the copolymer oxidized by ammonium persulfate exhibits the stepwise oxidation process of AP in PAP2 from the leucoemeraldine state to the emeraldine state, and then to the pernigraniline state. The structures of the copolymer at various oxidation states are depicted in Scheme 2. The LM copolymer has only one peak at ~330 nm representing benzenoid peak arising from $\pi$-$\pi^*$ transition in benzene unit. Further oxidation causes hypsochromic shifts of all peaks present in the spectrum and the appearance of a new peak at ~610 nm attributes to the transition $\pi b$-$\pi q$ from benzene ring to quinoid ring [34,35]. The intensity increase and the hypsochromic shift of this new peak with the oxidation process can be ascribed to the two-step oxidation from the leucoemeraldine state to the emeraldine state, and then to the perrigraniline state, which is in agreement with the two pairs of redox peaks in the cyclic voltammogram as shown in Fig. 4b. The first oxidation peak at 0.37 V corresponds to the transition from the leucoemeraldine to the emeraldine state, and the second peak at 0.82 V corresponds to the transition from the emeraldine to the perrigraniline state (as illustrated in Scheme 2). This is similar to the redox behavior of AP shown in Fig. 4a. All these spectroscopic and electrochemical results demonstrate the good electroactivity of the copolymers.

Fig. 5a–d shows the UV–visible spectra of the LM AP and three LM PAPs in DMF solutions. They all consist of one peak at ~330 nm attributable to the benzenoid ring absorption. It can be seen that this peak exhibits a blue shift from Fig. 5a–d, and the shift increases with the decrease of AP content in the copolymer. The benzenoid absorption region indicates the effective conjugation length of the AP segment, so we speculate that the blue shift could be due to the restriction of non-planar conformation of the AP backbone in the copolymers. The phenomenon might

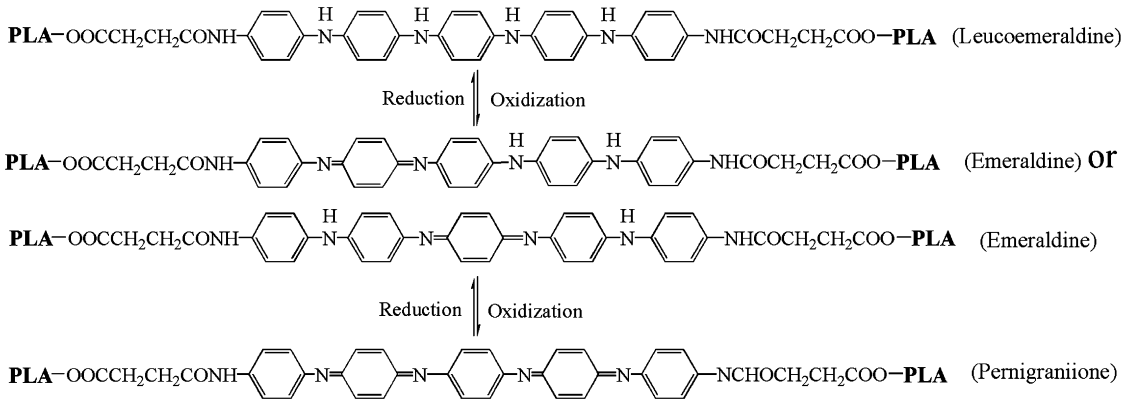


Scheme 2. Molecular structures of PAP copolymer at various oxidation states.

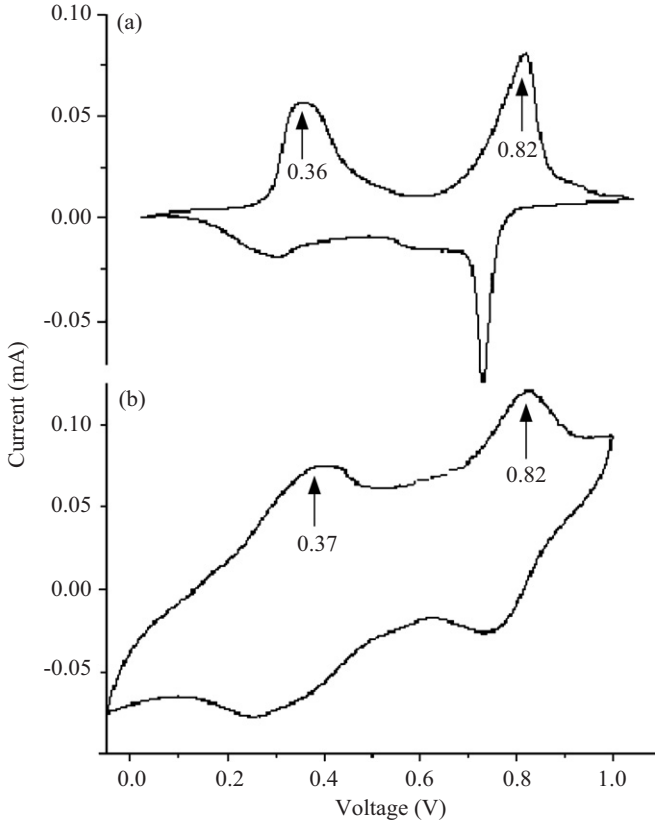


Fig. 4. The cyclic voltamograms of (a) AP and (b) PAP2 copolymer films on ITO glass in 1.0 M HCl using $Ag/Ag^{+}$ as reference electrode.

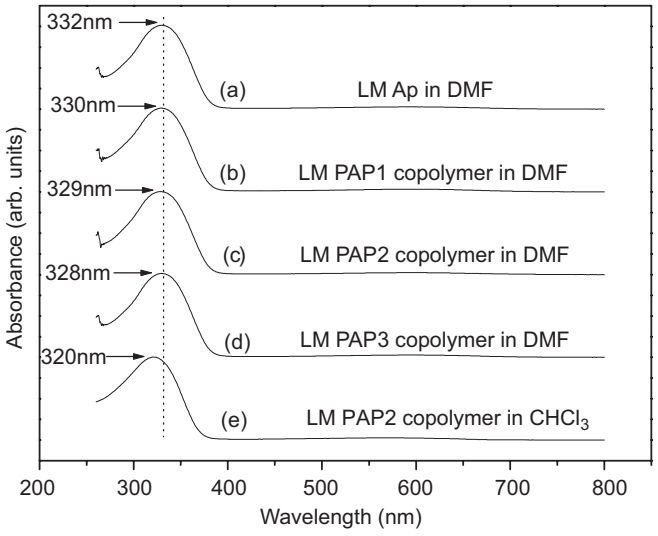


Fig. 5. UV–visible absorption spectra of: (a) LM AP, (b) LM PAP1, (c) LM PAP2, (d) LM PAP3 in DMF solutions, and of (e) LM PAP2 in $CHCl_3$ solution.

be caused by the incorporation of the long and flexible PLA chains, leading to the decrease in effective conjugation length of the AP. Moreover, longer the PLA chains are, greater the restriction of non-planar conformation appears to be. The UV–visible spectrum of the PAP2 in $CHCl_3$ solution is shown in Fig. 5e. Apparently, the absorption peak in $CHCl_3$ exhibits a blue shift compared to that in DMF solution. This may be related to the solubility of the copolymer in different solvents. Although the dissolution of the copolymers in $CHCl_3$ was improved over AP because of the PLA segments as discussed earlier, the solubility of AP segment remains poor. This could be regarded as pseudo dissolvability, meaning that the insoluble AP segments were forced by the PLA segments to disperse in $CHCl_3$. This pseudo dissolvability could explain the observation that there were no signals of AP segment in the NMR spectra of the PAP copolymers in $CDCl_3$. It may be also attributed to the strong restriction of planar conformation and to the decreased effective conjugation length of AP in the copolymers.

### 3.4. Electrical conductivity of the doped PAP copolymer film

The electrical conductivity of the PAP2 film doped with camphorsulfonic acid (CSA) and AP film doped with 1 M HCl were measured using the standard four-probe method. The electrical conductivity of PAP2 was $\sim 5 \times 10^{-6}$ S/cm, which is lower than that of AP films ($\sim 10^{-2}$ S/cm) but much higher than PLA ($< 10^{-8}$ S/cm) as expected.

Compared to AP, the reduction of conductivity of the copolymers is, obviously, owing to the less content of AP in the copolymer. It is difficult for an electron to transport from one polymer chain to another, that is, so-called "interchain transport" of electrons [40]. The AP segments in the copolymers were surrounded by PLA chains and there is little opportunity for AP segments to establish a channel for electron transition, leading to the conductivity drop. We are working on further increasing the conductivity of the copolymers by fine-tuning their nanostructures. On the other hand, it is possible that the conductivity of $\sim 5 \times 10^{-6}$ S/cm might be sufficient to conduct micro-current for stimulating neuronal cell proliferation and possibly differentiation because the micro-current intensity is very low in human body [41].

Fig. 6 shows the UV–visible spectra of PAP2 in DMF solutions at different oxidation states. Upon doping with CSA, the absorption spectrum (Fig. 6c) shows a characteristic polaron absorption peak at 442 nm and a localized polaron peak at 868 nm, together with the disappearance of the absorption peak at 598 nm and a continuous blue shift of the absorption peak at 330 nm as discussed in Fig. 6a and b. The strong localized absorbance peak at 868 nm results from the localization of the radical polaron along the doped copolymer backbone structure [42,43]. After the copolymer was doped, the extended chain conformation increases the conjugation length which leads to the delocalization of polarons. These results are consistent with the measurable conductivity of doped PAP copolymers.

To investigate to microstructure of copolymer, the TEM images of the PAP2 films prepared by ultracryotomy at −80 °C (Fig. 7a) and −60 °C (Fig. 7b) are shown. In Fig. 7a, the interlacement of the black particles corresponding to the AP segments and the white matrix contributing to the PLA segments in the image suggests the formation of micro-phase separation structure in the copolymer. We can see that the distribution of the white and black matrix is not very homogeneous, because the film prepared by ultracryotomy is not thin enough to achieve a monolayer of copolymer molecules for the brittleness of the sample at −80 °C, leading to the superposition of molecule layers. In fact, we speculate the interlaced distribution of the PLA segments and the AP segments is homogeneous. To confirm our supposition, another sample was prepared with thinner thickness at −60 °C and the copolymer chains in the film should be stretched along the cutting direction at this temperature. The arrow orientation in Fig. 7b represents the cutting direction and is perpendicular to the edge of the trace of cutting. The arrow head points to the edge of the trace of cutting in the top left corner of the image. The microstructure of stretched copolymer film clearly exhibits the homogeneous distribution of the interlacement of black and white stripes stretched from white particles and black micro-phase separating domains. The regular distribution of micro-phase structure may be formed by the assembly of triblock copolymer supporting the possibility of the conductivity of copolymer. The possible assembling process is shown in Scheme 3. The dispersion of copolymer chains in solvent is free and random (Scheme 3a), when the poor solvent is added in the system gradually, the AP segments are inclined to be aggregated due to the molecule interaction power, while the PLA segments are limited to be separated from AP (Scheme 3b). The gradual close packing of molecules is in fact a process of assembly. When the assembly reaches to a certain extent, the micro-phase separated morphology of the copolymer is formed as shown in Scheme 3c, which is in accordance with the morphology observed by TEM.

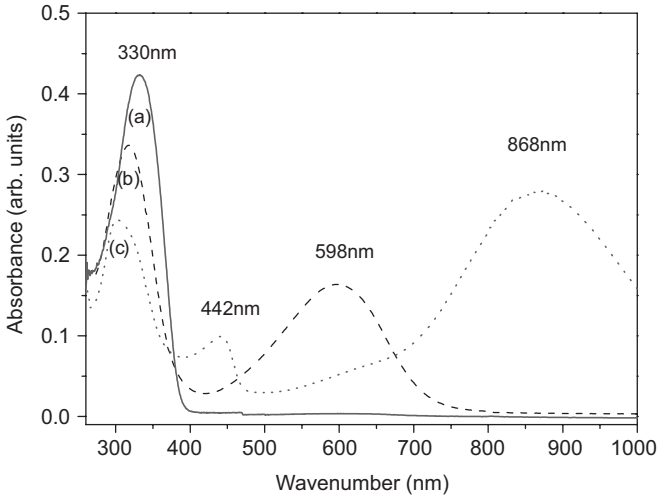


Fig. 6. UV–visible spectra of PAP2 copolymer in DMF in LM state (a), EM state (b) and (c) EM state doped with camphorsulfonic acid (CSA).

In the PAP copolymer, PLAs are the soft segments and AP is the hard segment. Such a soft-hard-soft structure of triblock copolymer has two advantages. First, the PLA chains are bonded on the two ends of the AP to increase its biocompatibility and apparent solubility. Second, this type of block copolymers could readily undergo self-assembly and form micro-phase separation. Thus, the soft PLA segments trend to aggregate together to form a continuous matrix, while the hard ones may form discontinuous domains. Within an AP domain the electric conduction is easy while between two adjacent domains the electric conduction might be realized through the tunnel effect through the PLA matrix. Therefore, the apparent conductivity is quite low.

### 3.5. *In vitro biodegradability of the PAP copolymer thin film*

The other critical feature of the PAP copolymer is its ability to degrade. The ester linkages, existed in the PLA segments and the PAP coplolymer, are known to be degradable. The *in vitro* degradation of PAP copolymer films in phosphate-buffered saline (PBS) at 37 °C is presented in Fig. 8. For the PAP copolymers, the degradation extent increased with the decrease of the PLA block length. Weight loss rate at 45 days was shown

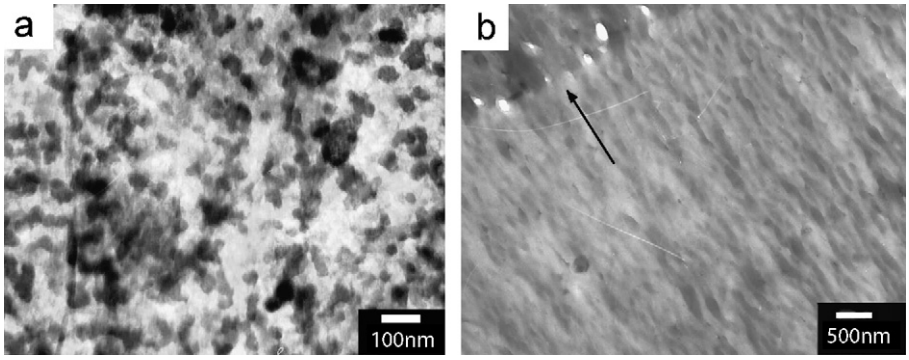


Fig. 7. TEM images of PAP2 films ultracryotomed at −80 °C (a) and −60 °C (b).

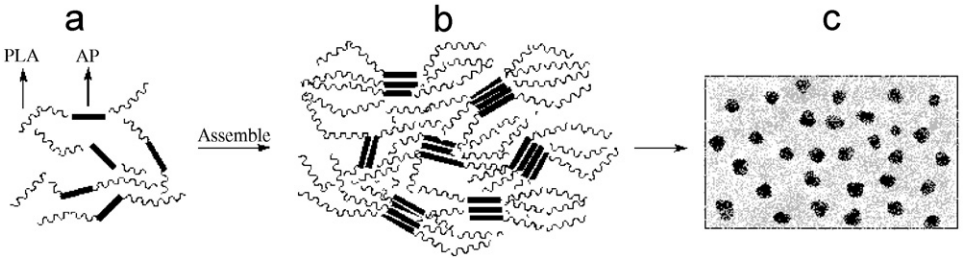


Scheme 3. Schematic illustration for the assembly of the PAP copolymer in solvent (a), adding the poor solvent (b), and the macroscopic morphology (c).

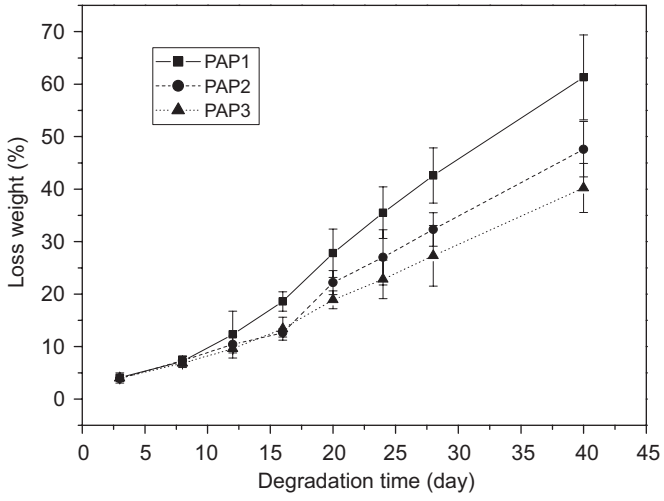


Fig. 8. Degradation of the PAP copolymers. Degradation studies of PAP films (10 × 10 × 0.4 mm) were performed in PBS (pH = 7.4) at 37 °C.

to be about 60% for the PAP1, which means the PLA segments almost fully degraded because of the very low molecular weight of the PLA blocks. Compared with PAP1 and PAP2, the degradation of the PAP3 copolymer was slow because of the longer molecular chains in PAP3 copolymer. The data above support the view that the PAP copolymers are indeed degradable.

### 3.6. Biocompability of the PAP copolymer

In the biomedical application, PAP copolymer should be non-toxic and able to support cell adhesion and growth. In order to assess the cell compatibility *in vitro*, the PAP2 copolymer and controlled tissue-culture-treated polystyrene (TCPS) are subjected to the biocompatibility with rat C6 glioma cells. The C6 cells provide a good measure of compatibility because they could exhibit their neural-like phenotype depending on cell–surface interactions. In Fig. 9, C6 cells are seeded and cultured for 4 and 48 h on the PAP2 copolymer thin film and TCPS surface, respectively. It can be seen that the C6 cells are well adhered to both of the PAP2 copolymer thin film (Fig. 9a) and TCPS surface (Fig. 9b), and readily exhibit their neural-like phenotype. The proliferation period of C6 cell is 24 h. After two proliferation period (48 h), the significant cell proliferations observed on the PAP2 copolymer thin film (Fig. 9c) are similar to control TCPS surface (Fig. 9d).

As shown in Fig. 10, the area fraction of C6 cells cultured for either 4 or 48 h on PAP2 copolymer is almost equal to TCPS and a little lower than TCPS. TCPS is famous for its good biocompatibility, and the similarity of the PAP2 copolymer to TCPS demonstrates that the PAP2 copolymer is non-toxic and can also support cell attachment and proliferation just like TCPS. The favorable biocompatibility of PAP2 copolymer is mainly attributed to the PLA segments which is of well-known biocompatibility.

## 4. Conclusions

A triblock copolymer, PLA-*b*-AP-*b*-PLA, containing one electroactive aniline pentamer (AP) center block and two bilateral biodegradable PLA (PLA) blocks has been

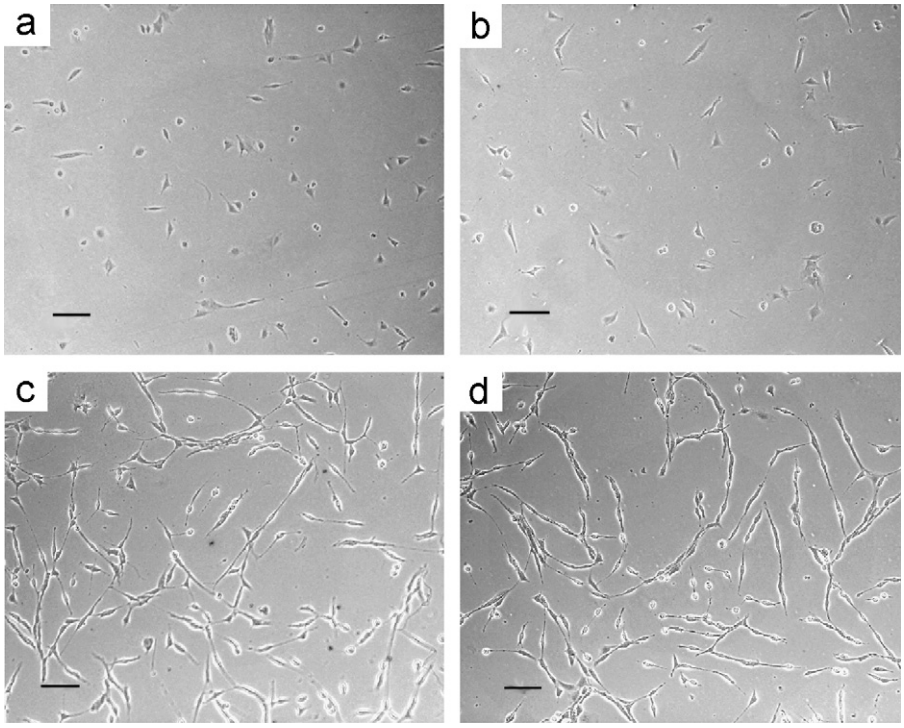


Fig. 9. Biocompatibility assessment with rat C6 glioma cells seeded on the PAP2 copolymer film (a) and TCPS surface (b) incubated for 4 h, the PAP2 copolymer film (c) and TCPS surface (d) incubated for 48 h. Scale bar = 100 μm.

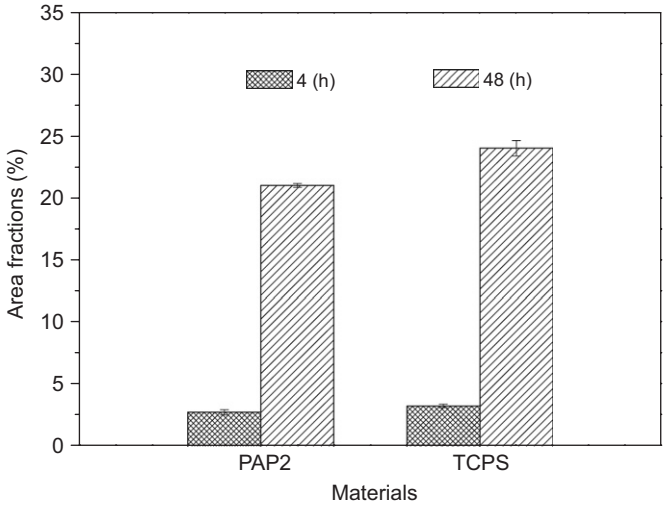


Fig. 10. Area fractions of the C6 cells adhered and proliferated on the surface of the PAP2 and TCPS films.

successfully synthesized. The copolymer exhibits much better solubility in common organic solvents than pure AP and polyaniline, which endow the copolymer with excellent thermomechanical property and processability for potential medical applications. The copolymer structure has been characterized by NMR, FT-IR, UV–visible spectroscopy, and GPC. Both UV–vis spectroscopy and cyclic voltammetry results show that the copolymer is electroactive. We also primarily investigated the degradability and biocompatibility of the copolymer, and proved that the PAP copolymer was degradable and supported cells attachment and proliferation. Further investigation is in vigorous progress to fabricate scaffolds from this copolymer for tissue engineering and to fully exploit the enhancing function to cell modalities of this electroactive copolymer system with electric stimulation. In addition, we are also studying the self-assembly of this copolymer in order to prepare nano-structured electroactive materials.

## Acknowledgments

Financial support was provided by the National Fund for the Distinguished Young Scholars (No: 50425309 to XSC), by International Cooperation Fund of Science and Technology (Key project 2005DFA50290) and by the Nanotechnology Institute of Southeastern Pennsylvania (YW, PIL and AGM). Y. Wei is most grateful to the Chinese Academy of Sciences for an Outstanding Overseas Scholar Award.

## References

[1] DeBerry DW. Modification of the electrochemical and corrosion behavior of stainless steels with an electroactive coating. J Electrochem Soc 1985;132:1022–6.
[2] Ahmad N, MacDiarmid AG. Inhibition of corrosion of steels with the exploitation of conducting polymers. Synth Met 1996;78:103–10.
[3] MacDiarmid AG, Mu SL, Somasiri NLD, Wu W. Electrochemical characteristics of 'polyaniline' cathodes and anodes in aqueous electrolytes. Mol Cryst Liq Cryst 1985;121:187–90.

[4] MacDiarmid AG, Yang LS, Huang WS, Humphrey BD. Polyaniline: electrochemistry and application to rechargeable batteries. Synth Met 1987;18:393–8.
[5] Sivaraman P, Hande VR, Mishra VS, Rao CS, Samui AB. All-solid supercapacitor based on polyaniline and sulfonated poly(ether ether ketone). J Power Sources 2003;124:351–4.
[6] Huang J, Virji S, Weiller BH, Kaner RB. Polyaniline nanofibers: facile synthesis and chemical sensors. J Am Chem Soc 2003;125: 314–5.
[7] Huang J, Virji S, Weiller BH, Kaner RB. Nanostructured polyaniline sensors. Chem Eur J 2004;10:1314–9.
[8] Anderson MR, Mattes BR, Reiss H, Kaner RB. Conjugated polymer films for gas separations. Science 1991;252:1412–5.
[9] Kaner RB. Gas, liquid and enantiomeric separations using polyaniline. Synth Met 2001;125:65–71.
[10] Huang SC, Ball IJ, Kaner RB. Polyaniline membranes for pervaporation of carboxylic acids and water. Macromolecules 1998; 31:5456–64.
[11] Trivedi DC, Dhawan SK. Grafting of electronically conducting polyaniline on insulating surfaces. Mater Chem 1992;2:1091–6.
[12] Maziarz EP, Lorenz SA, White TP, Wood TD. Polyaniline: a conductive polymer coating for durable nanospray emitters. J Am Soc Mass Spectrom 2000;11:659–63.
[13] Taka T. Emi-shielding measurements on poly(3-octyl thiophene) blends. Synth Met 1991;41:1177–80.
[14] Joo J, Epstein J. Electromagnetic- radiation shielding by intrinsically conducting polymers. Appl. Phys Lett 1994;65:2278–80.
[15] Wang CH, Dong YQ, Sengothi K, Tan KL, Kang ET. *In-vivo* tissue response to polyaniline. Synth Met 1999;102:1313–4.
[16] Schmidt CE, Venkatram RS, Vacanti J, Langer R. Stimulation of neurite outgrowth using an electrically conducting polymer. Proc Natl Acad Sci 1997;94:8948–53.
[17] Wei Y, Lelkes PI, MacDiarmid AG, Guterman E, Cheng S, Palouian K, et al. Electroactive polymers and nanostructured materials for neural tissue engineering. Peking University Press: Beijing; 2004. p. 430–436.
[18] Kamalesh S, Tan P, Wang J, Lee T, Kang ET, Wang CH. Biocompatibility of electroactive polymers in tissue. J Biomed Mater Res 2000;52:467–8.
[19] Guterman E, Cheng S, Palouian K, Bidez P, Lelkes PI, Wei Y. Peptide-modified electroactive polymers for tissue engineering applications. Polym Prepr 2002;43:766–7.
[20] Bidez P, Li S, MacDiarmid AG, Venancio EC, Wei Y, Lelkes PI. Polymaniline, an electroactive polymer, supports adhesion and proliferation of cardiac myoblasts. J Biomater Sci Polymer Edn 2006; 17:199–212.
[21] Kanatzidis MG. Conductive polymers. Chem Eng News 1990;68: 36–54.
[22] Street GB, Clarke TC. Conducting polymers: a review of recent work. IBM Journal of Research and Development 1981; 25: 51–7.
[23] Kotwal A, Schmidt CE. Electrical stimulation alters protein adsorption and nerve cell interactions with electrically conducting biomaterials. Biomaterials 2001;22:1055–64.
[24] Tiitu M, Hiekkataipale P, Hartikainen J, Makela T, Ikkala O. Viscoelastic and electrical transitions in gelation of electrically conducting polyaniline. Macromolecules 2002;35:5212–7.
[25] Li M, Guo Y, Wei Y, MacDiarmid AG, Lelkes PI. Electrospinning polyaniline-contained gelatin nanofibers for tissue engineering applications. Biomaterials 2006;27:2705–15.
[26] River TJ, Hudson TW, Schmidt CE. Synthesis of a novel, biodegradable electrically conducting polymer for biomedical applications. Adv Funct Mater 2002;12:33–7.
[27] Wang LX, Soczka-Guth T, Havinga E, Mullen K. Poly(phenylenesulfidephenylenamine) (PPSA)—The (''compound'') of polyphenylenesulfide with polyaniline. Angew Chem Int Ed Engl 1996;35:1495–7.
[28] Wang P, Tan KL. Synthesis and characterization of poly(ethylene glycol)-grafted polyaniline. Chem Mater 2001;13:581–7.
[29] Chen Y, Kang ET, Neoh KG, Tan KL. Chemical modification of polyaniline powders by surface graft copolymerization. Polymer 2000;41:3279–87.
[30] Wei Y, Li S, Jia X, Chen M, Mathai MW, Yeh J, et al. Synthesis of electroactive aniline oligomers of well-defined structures and their polymeric derivatives. Am Chem Soc Symp Ser 1999;24:384–98.
[31] Chao D, Lu X, Chen J, Zhao X, Wang L, Zhang W, et al. New method of synthesis of electroactive polyamide with amine-capped aniline pentamer in the main chain. J Polym Sci. Pol Chem 2006;44:477–82.
[32] Green TR, Fisher J, Matthews JB, Stone MH, Ingham E. Effect of size and dose on bone resorption activity of macrophages by *in vitro* clinically relevant ultra high molecular weight polyethylene particles. J Biomed Mater Res 2000;53:490–7.
[33] Cohn D, Hotovely Salomon A. Designing biodegradable multiblock PCL/PLA thermoplastic elastomers. Biomaterials 2005;26:2297–305.
[34] Chen L, Yu Y, Mao H, Lu X, Zhang W, Wei Y. Synthesis of amino-capped aniline pentamer and UV–Vis spectral study. Chem J Chinese U 2004;9:1768–70.
[35] Huang L, Hu J, Zhuang X, Ma J, Chen X, Jing X, et al. Synthesis and characterization of electrically active and biodegradable block copolymer-aniline pentamer and polylactide. Chem J Chinese U 2005;26:1771–3.
[36] Wang ZY, Yang C, Gao JP, Lin J, Meng XS. Electroactive polyimides derived from amino-terminated aniline trimer. Macromolecules 1998;31:2702–4.
[37] Putnam D, Langer R. Poly(4-hydroxy-L-proline ester): low-temperature polycondensation and plasmid DNA complexation. Macromolecules 1999;32:3658.
[38] Hong Z, Zhang P, He C, Qiu X, Liu A, Chen L, et al. Nanocomposite of poly(L-lactide) and surface grafted hydroxyapatite: mechanical properties and biocompatibility. Biomaterials 2005;26: 6296–304.
[39] Tang J, Jing X, Wang B, Wang F. Infrared spectra of soluble polyaniline. Synth Met 1988;24:231–8.
[40] Cheng D, Ng SC, Chan HSO. Morphology of polyaniline nanoparticles synthesized in triblock copolymers micelles. Thin Solid Films 2005;477:19–23.
[41] Niple JC, Daigle JP, Zaffanella LE, Sullivan T, Kavet R. A portable meter for measuring low frequency current in the human body. Bioelectromagnetics 2004;25:369–73.
[42] Gao J, Liu D, Samsinena J, Wang H. Synthesis and characterization of electrochromic polyamides with well-defined molecular structures and redox properties. Adv Funct Mater 2004;14:537–43.
[43] Cao Y, Smith P, Heeger AJ. Spectroscopic studies of polyaniline in solution and in spin-cast films. Synth Met 1989;32:263–81.